Dynamic Contrast-Enhanced Magnetic Resonance Imaging of Tumor-Induced Lymph Flow[1,2]

Alanna Ruddell[*], Maria I. Harrell[*],
Satoshi Minoshima[†], Kenneth R. Maravilla[†],
Brian M. Iritani[‡], Steven W. White[§]
and Savannah C. Partridge[†,§]

[*]Fred Hutchinson Cancer Research Center, Seattle, WA, USA; [†]Department of Radiology, University of Washington, Seattle, WA, USA; [‡]Department of Comparative Medicine, University of Washington, Seattle, WA, USA; [§]Seattle Cancer Care Alliance, Seattle, WA, USA

Abstract

The growth of metastatic tumors in mice can result in markedly increased lymph flow through tumor-draining lymph nodes (LNs), which is associated with LN lymphangiogenesis. A dynamic magnetic resonance imaging (MRI) assay was developed, which uses low–molecular weight gadolinium contrast agent to label the lymphatic drainage, to visualize and quantify tumor-draining lymph flow *in vivo* in mice bearing metastatic melanomas. Tumor-bearing mice showed greatly increased lymph flow into and through draining LNs and into the bloodstream. Quantitative analysis established that both the amount and the rate of lymph flow through draining LNs are significantly increased in melanoma-bearing mice. In addition, the rate of appearance of contrast media in the bloodstream was significantly increased in mice bearing melanomas. These results indicate that gadolinium-based contrast-enhanced MRI provides a noninvasive assay for high-resolution spatial identification and mapping of lymphatic drainage and for dynamic measurement of changes in lymph flow associated with cancer or lymphatic dysfunction in mice. Low–molecular weight gadolinium contrast is already used for 1.5-T MRI scanning in humans, which should facilitate translation of this imaging assay.

Neoplasia (2008) 10, 706–713

Introduction

The lymphatic system transports fluid and cells from the periphery to the circulation. This system is increasingly appreciated as a conduit for metastasis of a variety of human cancers including breast, colon, melanoma, and head and neck cancers (reviewed by Achen et al. [1] and Cao [2]). Tumor lymphatic vessel growth or lymphangiogenesis is often associated with metastasis and poor prognosis [3]. Moreover, studies of murine models have shown that vascular endothelial growth factor–induced lymphangiogenesis promotes tumor metastasis to lymph nodes (LNs) [4,5]. Thus, investigation of the lymphatic contribution to metastasis may to lead to diagnostic or therapeutic strategies to identify or prevent tumor dissemination.

Tumor metastasis is commonly diagnosed by examination of sentinel or tumor-draining lymph nodes (TDLNs) for the presence of tumor cells. However, an active involvement of the sentinel LN in tumor dissemination was not considered until the discovery that TDLNs can undergo extensive lymphangiogenesis [6,7]. This lymphatic sinus growth is associated with greatly increased lymph flow, detected by optical imaging of fluorescent nanoparticle or quantum dot accumulation within TDLNs in mice bearing B16-F10 melanomas [8] and in LNs from Eμ-c-*myc* transgenic mice developing B-cell lymphoma [7]. B-cell accumulation within the TDLN is required for LN lymphangiogenesis and for increased lymph flow [8]. Moreover, B-cell–deficient mice show reduced melanoma metastasis to LNs, supporting the idea that increased lymph flow through LNs

promotes tumor dissemination. Tumor vascular endothelial growth factor C overexpression can also stimulate lymph drainage from fibrosarcomas in part by increasing the number and size of tumor lymphatic vessels [9]. Such findings indicate dynamic alterations of lymph drainage in response to tumor growth, which could actively promote metastasis.

We sought to develop a more sensitive assay to analyze lymph drainage throughout the mouse, to further characterize tumor effects on lymph flow. Near infrared optical imaging shows promise for imaging superficial mouse lymph drainage; however, optical imaging is relatively low in resolution, and it does not detect deep lymphatic drainage basins [10,11]. Magnetic resonance imaging (MRI) provides superior three-dimensional (3D) resolution of surface or deep structures, and the lymphatic drainage can be labeled after injection of gadolinium contrast [12]. Therefore, we pursued an MRI strategy for murine lymphography (or lymphangiography). For lymphography, particles of 5 to 50 nm in diameter are generally used, because larger molecules are selectively taken up by and retained within lymphatic vessels [13]. A variety of experimental nanoparticles and dendrimers with these dimensions are being synthesized and tested for lymphography [14,15]. However, some gadolinium-based low–molecular weight contrasts such as dimeglumine gadopentate (Gd-DTPA) have been successfully used to identify lymphatic vessels and LNs in humans [16,17] and in dogs [18]. In addition, a recent report successfully used Gd-DTPA to image lymphatic vessels in the mouse tail [19], suggesting that low–molecular weight contrast agents may be useful for lymphography in mice.

In this study, we developed methods using low–molecular weight gadolinium contrast for high-resolution spatial mapping of lymph drainage in mice and for dynamic monitoring of lymph flow. We used the B16-F10 melanoma model for these studies, because we had found previously that implantation of B16-F10 cells into the rear footpad of syngeneic C57Bl/6 mice reliably increases lymph flow through the draining popliteal LN [8]. We determined that low–molecular weight Gd-DTPA makes an excellent MRI contrast for mouse lymphography, which allowed us to demonstrate significantly increased lymph flow into the tumor-draining lymphatic basin and then into the vascular circulation. Magnetic resonance imaging lymphography using low–molecular weight gadolinium contrast provides a useful tool for the localization and functional assessment of diseased or tumor-draining lymphatic vessels and LNs.

Methods

Mouse Tumor Model

Four-week-old C57BL/6J wild type mice were obtained from Jackson Laboratories (Bar Harbor, ME) and maintained in microisolator rooms at the Fred Hutchinson Cancer Research Center (FHCRC) animal facility under specific pathogen-free conditions. Experimental mice were injected in the left hind leg footpad with 200,000 B16-F10 cells (American Type Culture Collection, Manassas, VA) in 50 µl of Hanks' buffered saline solution (Gibco Life Technologies, Grand Island, NY), after testing to confirm that the cells were free of mycoplasma contamination (Cambrex, Rockland, MD). Mice were imaged at 20 to 23 days when tumors were 2 to 4 mm in diameter and were then killed by cervical dislocation. Experiments involving animals were approved by the FHCRC and University of Washington Animal Care and Use Committees.

Magnetic Resonance Image Acquisition

Mice were anesthetized with 2% to 3% isoflurane through an MR-compatible mobile inhalation system (DRE, Inc, Louisville, KY) and were positioned supine in a coil with 2% isoflurane maintenance. Coronal MR images were acquired on a 1.5-T clinical MRI system (Signa whole-body MRI scanner; General Electric Medical Systems, Milwaukee, WI) using a 2.5-cm-diameter solenoidal radiofrequency coil (built in-house) and a customized animal holder surrounded by 37°C heating pads (Braintree Scientific, Braintree, MA).

For lymphography, the dorsal toe of the rear foot was injected subcutaneously with 25 µl of Gd-DTPA (0.4 mM/kg Magnevist; Bayer Pharmaceuticals, Wayne, NJ). For angiography, 25 µl of Gd-DTPA was injected into the lateral tail vein. Contrast-enhanced imaging was performed using a coronal T1-weighted 3D fast gradient echo sequence [20]. The scanning protocol consisted of a high spatial resolution acquisition followed by two dynamic acquisitions before contrast injection and 10 postcontrast dynamic (high temporal resolution) 1-minute scans, followed by a final high spatial resolution acquisition. The high spatial resolution sequence was obtained using T_R = 15.5 milliseconds, T_E = 6.3 milliseconds, flip angle = 45°, field of view = 6 × 3 cm, imaging matrix = 256 × 160, slice thickness = 0.6 mm, number of excitations = 3, with approximately 42 slices for an acquisition time of 5 minutes 13 seconds. This sequence provided an in-plane image resolution of 0.2 mm. The dynamic sequence was obtained using T_R = 15.1 milliseconds, T_E = 6.3 milliseconds, flip angle = 45°, field of view = 6 × 3 cm, imaging matrix = 256 × 128, slice thickness = 0.8 mm, number of excitations = 1, with approximately 30 slices for an acquisition time of 59 seconds.

Image Analysis

Image analysis was performed using ImageJ software (National Institutes of Health, Bethesda, MD), with automation using Java-based software developed in-house. Regions of interest (ROIs) were calculated from T1-weighted 3D images by manually delineating ROIs on sequential MR images over one or more slices, and summing the volumes. For popliteal LN quantitation, the ROI was determined by inspection of precontrast slices to identify the popliteal fossa. Tumor-draining popliteal LNs were typically four times larger than normal [8], so that the ROI drawn was twice as large, and the number of slices measured was doubled from three to six slices for these LNs. Inguinal LNs were identified from postcontrast volumes. The same-size ROI was used over four slices for the similarly sized tumor-draining and control inguinal LNs. The integrated density (sum of the pixel values in selected postcontrast ROIs minus the sum of pixel values in precontrast ROIs) was then measured for each LN.

The central lymphatic vessel, right iliac blood vessels, and heart were quantified by drawing ROIs within each structure on a representative single slice at each time point, for pixel value measurement. The percent enhancement was calculated as the sum of the postinjection ROI pixel values minus the precontrast pixel values, divided by the precontrast values, multiplied by 100. Seven to nine tumor-bearing or control mice were analyzed in each group, and statistics were analyzed by 2-tailed Student's t-test. Blinded samples were independently evaluated by two observers, which yielded comparable results.

Volocity software (Improvision Inc, Waltham, MA) was used to construct 3D time-course movies. A 3D image of each slice stack was created using dynamic scans taken from 1 to 10 minutes after contrast injection, and the images were aligned sequentially over time.

Movies were converted to avi file format to permit Windows or Mac platform viewing.

Results

High-Resolution MRI Lymphography

Low–molecular weight gadolinium contrast was tested for high spatial resolution analysis of normal lymph drainage from the mouse hind leg. We previously characterized the lymph drainage of the mouse hind leg using Evans Blue dye injection [10]. The major lymphatic vessels drain into the popliteal or inguinal LNs, and then into the iliac plexus, iliac LNs, and other LNs traveling up the midline, before delivery into the subclavian vein and blood circulation [21], as illustrated in Figure 1A. Gd-DTPA contrast (Magnevist) was injected into the dorsal toe of the hind leg of anesthetized normal mice, followed by high-resolution image collection on a 1.5-T Signa clinical MRI scanner.

High-resolution maximum intensity projection (MIP) images of a normal mouse 25 to 30 minutes after contrast injection into the dorsal toe (Figure 1B, arrow) reveal labeling of the major leg lymphatic vessels entering the popliteal or inguinal LNs (Figure 1B, arrowheads). Contrast continued traveling through the iliac plexus and then up the midline through the iliac, renal, and para-aortic LNs toward the heart (Figure 1B, "H"). The contrast-enhanced vessel abruptly terminated at the heart, presumably because the contrast was greatly diluted as it entered the blood circulation. These contrast-enhanced vessels and LNs were readily distinguished from background, shown in a precontrast image (Figure 1C). Thus, the
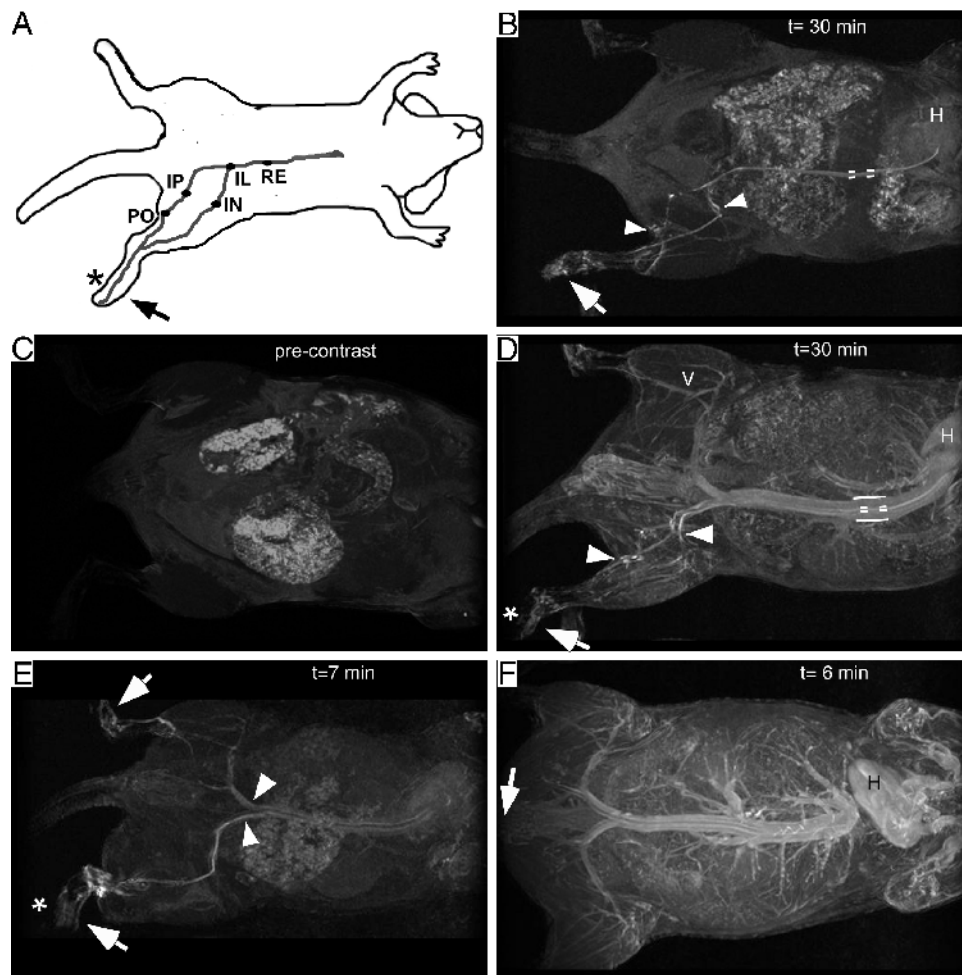

Figure 1. High-resolution MRI lymphography demonstrates tumor-induced lymph drainage. (A) Map of hind foot lymph drainage through major lymphatic vessels (gray) and LNs (black circles). *IL* indicates iliac LN; *IN*, inguinal LN; *IP*, iliac plexus; *PO*, popliteal LN; *RE*, renal LN. (B) High-resolution MIP of the control mouse 30 minutes after injection of Gd-DTPA into the dorsal toe (arrow) of the hind leg labels popliteal and inguinal nodes (arrowheads), central lymphatic vessel and LNs (dashed line), and lymph drainage into the heart ("H") in a normal mouse. (C) High-resolution precontrast MIP of mouse before Gd-DTPA injection. (D) High-resolution MIP of tumor-bearing mouse 30 minutes after injection of Gd-DTPA into the dorsal toe (arrow) of the tumor-draining foot (asterisk). Popliteal and inguinal LNs are labeled (arrowheads), and the contrast has reached the heart and traveled through to the vascular circulation on the contralateral side ("V"). The wide vena cava and aorta are labeled (solid lines) as well as the thin central lymphatic vessel (dashed line). (E) Toes on both legs of a mouse bearing a tumor in the left hind foot (asterisk) were injected simultaneously (arrows), highlighting the lymphatic vessels on both sides of the animal at 7 minutes after contrast injection. Lymph drainage is greatly increased from the tumor-bearing leg. Note that two thin central lymphatic vessels are labeled when both hind legs are injected with contrast (arrowheads). (F) Imaging at 6 minutes after intravenous tail vein injection identifies blood vessels of tumor-bearing mouse.

Gd-DTPA contrast appeared to label major afferent and efferent lymphatic vessels and LNs draining the foot, and extending all the way up the midline to empty into the bloodstream. Moreover, the lymphatic vessels and LNs identified by contrast-enhanced MRI lymphography match those identified by Evans Blue dye injection [10].

Tumor-Induced Lymph Flow

B16-F10 melanomas grown in the rear footpad increase lymph drainage through the popliteal LN at early stages within 3 weeks after implantation, despite the small size of these tumors [8]. Gadolinium contrast-enhanced MRI was performed after dorsal toe injection to characterize this tumor-induced lymph flow. The pattern of lymph labeling in these mice (Figure 1D) was very different from that observed in control mice at 30 minutes after the injection of contrast (Figure 1B). In addition to strong labeling of the tumor-draining lymphatic vessels and LNs, Gd-DTPA labeled the heart and blood vessels. This is indicated by the appearance of a thick line representing the vena cava and aorta traveling along the midline (Figure 1D, lines), which is distinct from the thinner central lymphatic vessel and LNs (Figure 1D, dashed lines). Smaller blood vessels throughout the body also were labeled and were readily identified in the uninjected contralateral leg of tumor-bearing mice (Figure 1D, "V"). These findings indicate that the footpad melanoma greatly increases lymph flow from the tumor through into the blood circulation.

Although our initial analysis using near infrared optical imaging only revealed increased lymph flow within the tumor-draining popliteal LN [8], high-resolution MRI suggests major enhancement of lymph drainage that can be detected from the foot tumor through draining LNs, and extending all the way into the bloodstream. This finding was confirmed by simultaneous injection of Gadolinium into both rear toes of tumor-bearing mice, which demonstrated that lymph drainage is selectively increased in the tumor-draining leg (Figure 1E). Thus, the melanoma exerts long-distance effects on lymph drainage from the footpad tumor through the draining LN and on into the circulation, without affecting the lymph drainage of the normal contralateral leg.

Comparison of Contrast-Enhanced Lymphography and Angiography

The Gd-DTPA contrast has low molecular weight, so that it could potentially enter the blood circulation directly in addition to traveling through the lymphatics. We used several approaches to determine whether the labeled vessels are lymphatic or vascular and to assess the contribution of vascular uptake to the contrast enhancement observed. First, Gd-DTPA injection into the dorsal toe of both feet of a tumor-bearing mouse demonstrated two central lymphatic vessels (Figure 1E, arrowheads), whereas injection of one leg labeled only one central lymphatic vessel (Figure 1B, dashed line), as would be predicted for specific labeling of the paired lymphatic vessels traveling up the midline. These narrow central lymphatic vessels (Figure 1D, dashed lines) are distinct from the lightly labeled and wider aorta and vena cava (Figure 1D, bars). The lymphatic vessel pattern identified by toe subcutaneous injection (Figure 1B) is also distinct from the blood vessel pattern identified by intravenous tail vein injection, which labels the vena cava and aorta on the midline and smaller blood vessels throughout the mouse (Figure 1F). Thus, low–molecular weight Gd-DTPA selectively labels lymphatic vessels after subcutaneous injection, or blood vessels after intravenous injection, provided that the mice are imaged soon after contrast injection.

Dynamic Imaging of Tumor Lymph Drainage

The kinetics of lymph drainage were examined by taking rapid scans every minute for the first 10 minutes after Gd-DTPA injection, to obtain a time course of contrast flow. Dynamic MIP images from tumor-bearing versus control mice show major differences in the rate and amount of lymph flow after injection (Figure 2). Within 1 minute after injection, the tumor-bearing mouse showed contrast labeling up through the draining LNs (Figure 2D), relative to the precontrast image (Figure 2B). This lymphatic pattern of contrast in tumor-bearing mice intensified through 9 minutes after injection when Gd-DTPA then also labeled the heart, vena cava, and blood vessels of the uninjected contralateral hind leg (Figure 2H). In the control mouse, the contrast weakly labeled the draining LNs and did not appreciably enter the vascular circulation even at 9 minutes after injection (Figure 2G). These findings demonstrate that the tumor greatly increases the rate of lymphatic drainage.

Movies were generated from dynamic scans of the same control and tumor-bearing mice imaged in Figure 2 and were processed using the Volocity software to generate a 3D image over time. These movies confirmed that lymph flows continuously from the injected foot through draining LNs and on up the midline to the heart in normal mice (Figure W1). The movie of the tumor-bearing mouse illustrated increased lymph flow from the foot to draining LNs, and then up the midline to the heart and blood circulation (Figure W2). Interestingly, there was no obvious difference in the number, pattern, or diameter of lymphatic vessels in tumor-bearing or control mice, although the popliteal LN draining the tumor was four times larger than normal [8]. The mechanism by which B16-F10 melanomas increase regional lymph drainage remains to be determined.

Quantification of Tumor-Induced Lymph Flow

The tumor-induced lymph flow alterations were further investigated using quantitative analysis to examine the amount and rate of contrast transport. The NIH ImageJ software was used to perform volumetric image analysis of the dynamic scans, compiled from images taken over the first 8 minutes after contrast injection of tumor-bearing or control mice. Regions of interest were drawn over lymphatic and vascular structures in slices from these volumes, and the contrast signal was measured at each time point. The integrated density was measured by summing pixel values in the postcontrast ROIs and subtracting the sum of precontrast pixel values. For the assessment of popliteal LNs, the fossa was readily identified in precontrast images, as illustrated by the ROI drawn in Figure 3A. Three slices were required to include all of the popliteal fossa in normal mice. However, the popliteal LN is four times larger than normal in tumor-bearing mice [8] so that the ROI size was doubled, and the number of slices analyzed were doubled to six slices for tumor-draining popliteal LNs. The inguinal LN was identified after labeling with contrast, so that postcontrast images were used to draw an ROI over the inguinal LN, as illustrated in Figure 3B. The volume of the tumor-draining inguinal LN was not significantly increased, so that equally sized ROIs drawn over the inguinal LN were analyzed in four slices each from tumor-bearing or control mice.

The integrated density values from tumor-draining left popliteal LNs increased much more rapidly than values from control popliteal LNs, and this increase was statistically significant from 3 to 8 minutes after injection (Figure 4A, left panel). Measurement of contrast signal from 0 to 4 minutes demonstrated a fourfold increase in the rate of
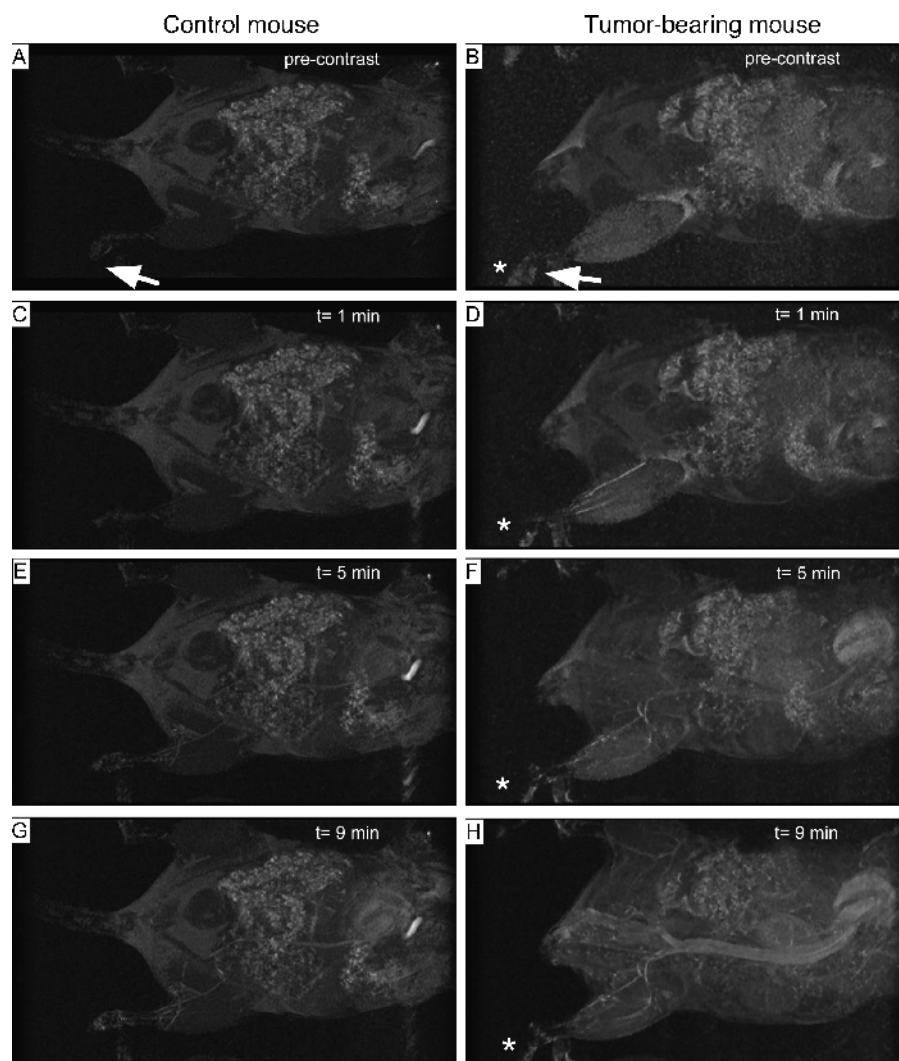
Figure 2. Dynamic MRI analysis of tumor-induced lymph flow. Low-resolution MRI before and after injection of Gd-DTPA into the dorsal toe (arrow) of a control mouse (left column) and a mouse bearing a tumor in the left hind foot (right column, asterisk indicates the location of tumor). Dynamic images before injection (A, control; B, tumor-bearing) and at 1 (C, control; D, tumor-bearing), 5 (E, control; F, tumor-bearing), and 9 minutes (G, control; H, tumor bearing) after injection.

enhancement of contrast in the tumor-draining left popliteal LN, which was also statistically significant (Figure 4A, *right panel*).

Lymph flow through the popliteal LN of the uninjected right hind leg was also measured to determine how much of the popliteal LN signal is contributed by vascular spread of contrast into the uninjected leg. The uptake of contrast into the right popliteal LN was very low in tumor-bearing or control mice, and the rate of enhancement was negligible in both cases (Figure 4B). These results confirm that subcutaneous injection of Gd-DTPA contrast specifically detects lymph flow, with negligible labeling of LN blood vessels at early time points.

Quantification of contrast enhancement in the left tumor-draining inguinal LN showed greatly increased lymph flow relative to control inguinal LNs, and this increase was statistically significant from 1 to 4 minutes after injection (Figure 4C, *left panel*). The rate of contrast enhancement from 0 to 4 minutes was also significantly increased in tumor-draining inguinal LNs (Figure 4C, *right panel*). The tumor-draining inguinal LN was only slightly enlarged, so that tumor-induced lymph flow does not require LN enlargement. The inguinal LN seems to provide the major lymphatic drainage for the mouse

hind leg, because much more contrast signal was detected in the tumor-draining inguinal LN (Figure 4C, *left panel*) than in the popliteal LN (Figure 4A, *left panel*).

Tumors Increase Lymph Drainage into the Blood Stream

The growing B16-F10 melanomas seem to not only enhance lymph flow through draining LNs, but they also increase lymph delivery into the vascular circulation. The kinetics of contrast accumulation in the central lymphatic vessel draining the midline, the heart, and the right iliac blood vessels were measured to assess whether the rate of entry of lymph contrast into the bloodstream is significantly increased in tumor-bearing mice. Regions of interest were drawn over representative regions, and contrast signal was measured in a single slice. These area-independent measurements were expressed as percent enhancement (sum of postinjection ROI pixel values minus precontrast pixel values, divided by precontrast values, × 100). An ROI was drawn over a representative slice showing the central lymphatic vessel below the heart (as illustrated in Figure 3C). This analysis demonstrated increased lymph flow through the central lymphatic
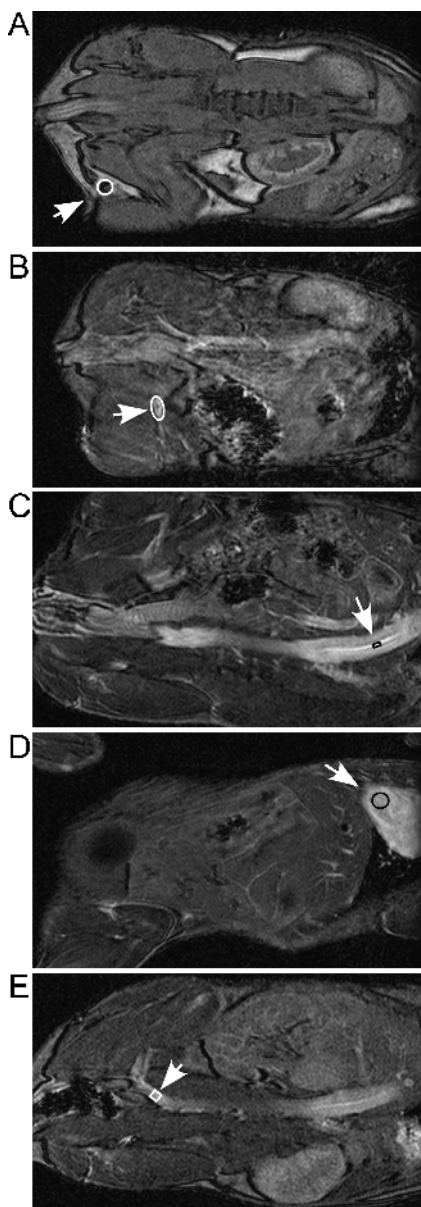
Figure 3. Identification of lymphatic and vascular structures for contrast measurement. Representative ROIs drawn for measurement of pixel values are outlined on single-slice images and are identified using arrows. (A) Popliteal fossa in precontrast image. (B) Inguinal LN iROI in a postcontrast image. (C) Central lymphatic vessel ROI in a postcontrast image. (D) Heart ROI in a postcontrast image from intravenously injected mouse. (E) Iliac blood vessel ROI in a postcontrast image.

vessels of tumor-bearing mice, which was significantly higher than normal from 1 to 3 minutes after contrast injection (Figure 5A).

Entry into the vascular system was assessed by measuring percent enhancement of a representative ROI in a single slice of the heart (Figure 3D) or right iliac blood vessels (Figure 3E). Contrast was significantly increased in the heart from 2 to 5 minutes after injection in tumor-bearing mice (Figure 5B). Contrast appearance in the iliac blood vessels was further delayed, so that it showed significant increases in tumor-bearing mice from 3 to 6 minutes after injection (Figure 5C). Thus, tumor-induced lymph drainage not only increases the amount and rate of lymph flow through the lymphatic

system, but also delivers lymph into the bloodstream at an increased rate, which can be quantified by dynamic MRI and image analysis.

Discussion

A dynamic contrast-enhanced MRI lymphography assay was developed in mice, which identified extensive alterations in lymph drainage induced by metastatic melanomas. Tumor growth in the footpad was associated with increased lymph flow from the rear leg through a series of draining LNs and resulted in accelerated contrast delivery into the heart and vascular circulation. Tumor-induced lymph drainage involved an increase in both the amount and the rate of lymph transport. Tumor-derived signals direct this increased flow, because increased lymph drainage was restricted to the tumor lymphatic drainage basin.

The mechanism by which tumors increase lymph flow is not yet understood. Early-stage B16-F10 melanomas do not induce lymphangiogenesis (or angiogenesis) within the ventral footpad tumor or the dorsal toe where the contrast was injected [8]. Our MRI studies demonstrated that there was no obvious increase in the number, size, or pattern of major leg-draining lymphatic vessels. Instead, the major physical alteration in the tumor-draining leg was the fourfold enlargement of the tumor-draining popliteal LN [8]. In addition, the
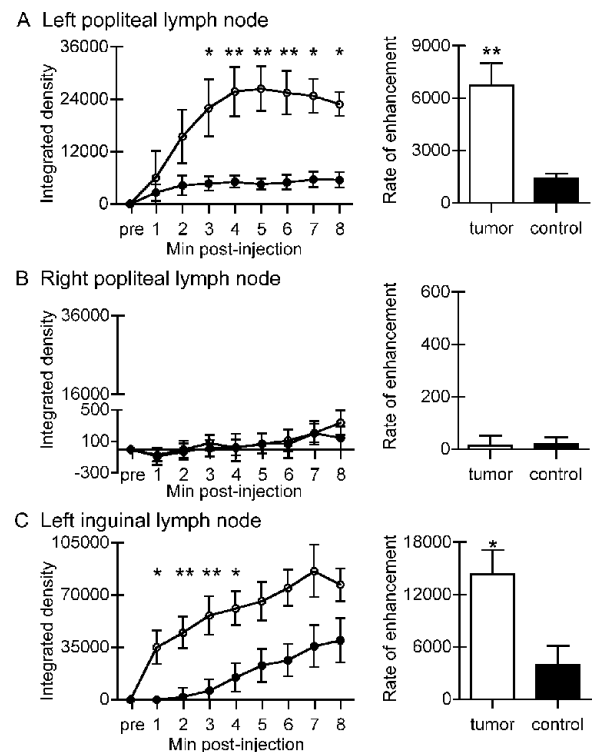

Figure 4. Increased amount and rate of lymph flow through tumor-draining LNs. The integrated density of Gd-DTPA contrast within ROIs in the tumor-draining left popliteal (A) and inguinal LNs (C) is increased in tumor-draining LNs (white circles) relative to control LNs (black circles; $*P < .04$, $**P < .004$, $N = 7$). In contrast, the integrated density of Gd-DTPA signal in the nondraining right popliteal LN does not significantly increase relative to normal (B). The rate of enhancement of Gd-DTPA signal (average increase in integrated density per minute) in the first 4 minutes is significantly increased in the tumor-draining left popliteal (A) and inguinal LNs (C) but not in the right popliteal LN (B). Standard errors are shown.
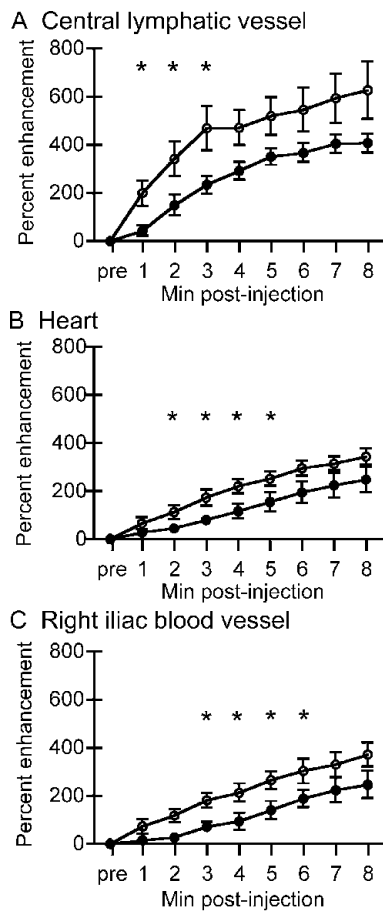
Figure 5. Tumor-induced lymph flow accelerates contrast arrival in the bloodstream. (A) The percent enhancement of Gd-DTPA over the central lymphatic vessel is significantly faster in tumor-bearing mice (white circles) relative to control mice (black circles) at 1 to 3 minutes after injection (*$P < .04$, $N = 7$). (B) Contrast enhancement in the heart is significantly increased at 2 to 5 minutes in tumor-bearing mice compared to control mice. (C) The percent enhancement in the right iliac blood vessels is significantly increased at 3 to 6 minutes in tumor-bearing mice relative to control mice. Standard errors are shown.

lymphatic sinuses within these tumor-draining popliteal LNs increased ninefold [8]. The tumor-draining inguinal LN showed a more moderate increase in diameter, whereas it also exhibited extensive lymphangiogenesis (data not shown). Thus, the major alterations associated with tumor-induced lymph flow are lymphangiogenesis and enlargement of TDLNs, supporting the idea that these LNs have an active role in tumor-induced lymph flow [7,8]. Lymph node enlargement or tumor-reactive lymphadenopathy is commonly observed in human cancer patients [22], suggesting that lymph flow through draining LNs could also increase in human cancer patients. Further studies will investigate the contribution of LNs to normal variations in lymph drainage and to tumor-induced lymph flow.

Our findings are consistent with the hypothesis that LN lymphangiogenesis and tumor-induced lymph flow actively drive metastasis into and through draining LNs [7,8]. This MRI study demonstrates that accelerated lymph flow is sustained throughout the lymphatic drainage of the tumor, which could not only promote spread of primary footpad tumors into the popliteal or inguinal TDLN but also stimulate secondary lymphatic dissemination to the draining iliac

LN, which is sometimes observed in mice bearing popliteal LN metastases (data not shown). Further evidence that LN alterations promote metastasis comes from the finding that mutations in the p53 or p19/Arf tumor suppressors selectively drive LN lymphangiogenesis and dissemination of squamous cell carcinomas to draining LNs and to the lungs [23]. Lymph node lymphangiogenesis and increased tumor-draining lymph flow could predict metastatic potential; however, these changes could alternatively represent a general feature of cancers in mice. Further investigations will determine the potential of tumor-induced lymph flow to predict metastatic potential or to identify cancer in mice or in humans.

Low–molecular weight gadolinium contrast agents were thought to be unsuitable for lymphography in the mouse due to their rapid diffusion out of lymphatic vessels, although they have been successfully used for lymphography in larger animals [18,24] and in humans [17,25]. In fact, Gd-DTPA fails to preferentially label lymphatics in mice imaged at later times after injection [14,26]. However, we found that Gd-DTPA makes an excellent contrast agent for kinetic analysis of lymph flow in mice when they are imaged soon after injection. We did not identify significant leakage out of lymphatic vessels during short-term imaging. Moreover, this small-molecule contrast was specifically taken up by the lymphatic vessels after subcutaneous injection and did not significantly enter the blood circulation until the lymph reached the heart. These findings are in agreement with reports of selective lymph uptake after subcutaneous lymphography in human patients [27].

The efficient uptake of low–molecular weight Gd-DTPA into the lymphatic system is advantageous for labeling and quantitative analysis of normal lymphatic vessels and LNs immediately after injection, whereas larger nanoparticles label the lymphatic system much more slowly [14]. This dynamic MRI scanning strategy using low–molecular weight contrast can be used to quantitate lymph flow from the peripheral lymphatic vessels on through the blood circulation. The lymph drainage basins analyzed can be specified depending on the location of the subcutaneous injection [28], so that analysis of most anatomic regions should be feasible by MRI lymphography. Pilot studies have not identified toxicity after subcutaneous injection of low–molecular weight gadolinium contrast for 1.5-T MRI in human subjects [16,17]. However, intravenously injected gadolinium contrast agents have been associated with nephrogenic systemic fibrosis in patients with impaired renal function, so that these potential complications should be considered when using gadolinium contrast [29].

Magnetic resonance imaging lymphography identified tumor-induced lymph flow from the foot into the heart and blood circulation. This assay may therefore be useful not only for the identification and mapping of sentinel LNs [17,25] but also for the diagnosis of tumor-associated changes in lymph flow. Bilateral contrast injection could allow internally controlled comparison of lymph flow in the control *versus* tumor-draining sides of the body, as was performed for some of the mice in this study. The kinetics of contrast appearance in the bloodstream could also be used as an indirect measure of lymph drainage. Dynamic contrast-enhanced MRI assessment of tumor-induced lymph flow could complement other MRI strategies being developed for cancer diagnosis, such as analysis of LN uptake of iron nanoparticles in macrophages [30] or iron nanoparticle labeling of tumor cells in mice [31]. Magnetic resonance imaging lymphography may also be useful for the analysis of experimental lymphedema or lymphatic malformations in mice [32,33]. Thus, the MRI lymphography assay we have developed should allow detailed anatomic and quantitative assessment

of lymph transport throughout the lymphatic system, in cancer and other diseases in mice, with potential for translation to humans.

References

[1] Achen M, Mann G, and Stacker S (2006). Targeting lymphangiogenesis to prevent tumour metastasis. *Br J Cancer* **94**, 1355–1360.

[2] Cao Y (2005). Emerging mechanisms of tumour lymphangiogenesis and lymphatic metastasis. *Nat Rev Cancer* **5**, 735–743.

[3] Sundar SS and Ganesan TS (2007). Role of lymphangiogenesis in cancer. *J Clin Oncol* **25**, 4298–4307.

[4] Achen M, McColl B, and Stacker S (2005). Focus on lymphangiogenesis in tumor metastasis. *Cancer Cell* **7**, 121–127.

[5] He Y, Karpanen T, and Alitalo K (2004). Role of lymphangiogenic factors in tumor metastasis. *Biochim Biophys Acta* **1654**, 3–12.

[6] Hirakawa S, Kodama S, Kunstfeld R, Kajiya K, Brown LF, and Detmar M (2005). VEGF-A induces tumor and sentinel lymph node lymphangiogenesis and promotes lymphatic metastasis. *J Exp Med* **201**, 1089–1099.

[7] Ruddell A, Mezquita P, Brandvold KA, Farr A, and Iritani BM (2003). B lymphocyte–specific c-Myc expression stimulates early and functional expansion of the vasculature and lymphatics during lymphomagenesis. *Am J Pathol* **163**, 2233–2245.

[8] Harrell MI, Iritani BM, and Ruddell A (2007). Tumor-induced sentinel lymph node lymphangiogenesis and increased lymph flow precede melanoma metastasis. *Am J Pathol* **170**, 774–786.

[9] Hoshida T, Isaka N, Hagendoorn J, di Tomaso E, Chen YL, Pytowski B, Fukumura D, Padera TP, and Jain RK (2006). Imaging steps of lymphatic metastasis reveals that vascular endothelial growth factor-C increases metastasis by increasing delivery of cancer cells to lymph nodes: therapeutic implications. *Cancer Res* **66**, 8065–8075.

[10] Harrell MI, Iritani BM, and Ruddell A (2007). Lymph node mapping in the mouse. *J Immunol Methods* **332**, 170–174.

[11] Kwon S and Sevick-Muraca EM (2007). Noninvasive quantitative imaging of lymph function in mice. *Lymphat Res Biol* **5**, 219–232.

[12] Pathak AP, Bhujwalla ZM, and Pepper MS (2004). Visualizing function in the tumor-associated lymphatic system. *Lymphat Res Biol* **2**, 165–172.

[13] Swartz MA (2001). The physiology of the lymphatic system. *Adv Drug Deliv Rev* **50**, 3–20.

[14] Kobayashi H, Kawamoto S, Star RA, Waldmann TA, Tagaya Y, and Brechbiel MW (2003). Micro-magnetic resonance lymphangiography in mice using a novel dendrimer-based magnetic resonance imaging contrast agent. *Cancer Res* **63**, 271–276.

[15] Melancon MP, Wang Y, Wen X, Bankson JA, Stephens LC, Jasser S, Gelovani JG, Myers JN, and Li C (2007). Development of a macromolecular dual-modality MR-optical imaging for sentinel lymph node mapping. *Invest Radiol* **42**, 569–578.

[16] Lohrmann C, Foeldi E, Bartholomae JP, and Langer M (2007). Gadoteridol for MR imaging of lymphatic vessels in lymphoedematous patients: initial experience after intracutaneous injection. *Br J Radiol* **80**, 569–573.

[17] Ruehm SG, Schroeder T, and Debatin JF (2001). Interstitial MR lymphography with gadoterate meglumine: initial experience in humans. *Radiology* **220**, 816–821.

[18] Suga K, Yuan Y, Ogasawara N, Okada M, and Matsunaga N (2003). Visualization of normal and interrupted lymphatic drainage in dog lets with interstitial MR lymphography using an extracellular MR contrast agent, gadopentate dimeglumine. *Invest Radiol* **38**, 349–358.

[19] Pan D, Suzuki Y, Yang PC, and Rockson SG (2006). Indirect magnetic resonance lymphangiography to assess lymphatic function in experimental murine lymphedema. *Lymphat Res Biol* **4**, 211–216.

[20] Wilmes LJ, Pallavicini MG, Fleming LM, Gibbs J, Wang D, Li KL, Partridge SC, Henry RG, Shalinsky DR, Hu-Lowe D, et al. (2007). AG-013736, a novel inhibitor of VEGF receptor tyrosine kinases, inhibits breast cancer growth and decreases vascular permeability as detected by dynamic contrast-enhanced magnetic resonance imaging. *Magn Reson Imaging* **25**, 319–327.

[21] Tilney NL (1971). Patterns of lymphatic drainage in the adult laboratory rat. *J Anat* **109**, 369–383.

[22] Ioachim HL and Ratech H (2002). *Ioachim's Lymph Node Pathology.* Philadelphia, PA: Lippincott Williams and Wilkins.

[23] Ruddell A, Kelly-Spratt KS, Furuya M, Parghi SS, and Kemp CJ (2007). p19/Arf and p53 suppress sentinel lymph node lymphangiogenesis and carcinoma metastasis. *Oncogene* [E-pub ahead of print]. doi:10.1038/sj.onc.1210973.

[24] Ruehm S, Corot C, and Debatin J (2001). Interstitial MR lymphography with a conventional extracellular gadolinium-based agent: assessment in rabbits. *Radiology* **218**, 664–669.

[25] Suga K, Yuan Y, Ogasawara N, Okada M, and Matsunaga N (2003). Localization of breast sentinel lymph nodes by MR lymphography with a conventional gadolinium contrast agent. *Acta Radiol* **44**, 35–42.

[26] Mounzer R, Shkarin P, Papademetris X, Constable T, Ruddle NH, and Fahmy TM (2007). Dynamic imaging of lymphatic vessels and lymph nodes using a bimodal nanoparticulate contrast agent. *Lymphat Res Biol* **5**, 151–158.

[27] Lohrmann C, Foldi E, Bartholoma JP, and Langer M (2006). MR imaging of the lymphatic system: distribution and contrast enhancement of gadodiamide after intradermal injection. *Lymphology* **39**, 156–163.

[28] Kobayashi H, Hama Y, Koyama Y, Barret T, Regino CA, Urano Y, and Choyke PL (2007). Simultaneous multicolor imaging of five different lymphatic basins using quantum dots. *Nano Lett* **7**, 1711–1716.

[29] Ersoy H and Rybicki FJ (2007). Biochemical safety profiles of gadolinium-based extracellular contrast agents and nephrogenic systemic fibrosis. *J Magn Reson Imaging* **26**, 1190–1197.

[30] Harisinghani M, Ross RW, Guimaraes AR, and Weissleder R (2007). Utility of a new bolus-injectable nanoparticle for clinical cancer staging. *Neoplasia* **9**, 1160–1165.

[31] Foster PJ, Dunn EA, Karl KE, Snir JA, Nycz CM, Harvey AJ, and Pettis RJ (2008). Cellular magnetic resonance imaging: *in vivo* imaging of melanoma cells in lymph nodes of mice. *Neoplasia* **10**, 207–216.

[32] Dellinger MT, Hunter RJ, Bernas MJ, Witte MH, and Erickson RP (2007). Chy-3 mice are VEGF-C haploinsufficient and exhibit defective dermal superficial to deep lymphatic transition and dermal lymphatic hypoplasia. *Dev Dyn* **236**, 2346–2355.

[33] Tammela T, Saaristo A, Holopainen T, Lyytikkä J, Kotronen A, Pitkonen M, Abo-Ramadan U, Ylä-Herttuala S, Petrova TV, and Alitalo K (2007). Therapeutic differentiation and maturation of lymphatic vessels after lymph node dissection and transplantation. *Nat Med* **13**, 1458–1466.
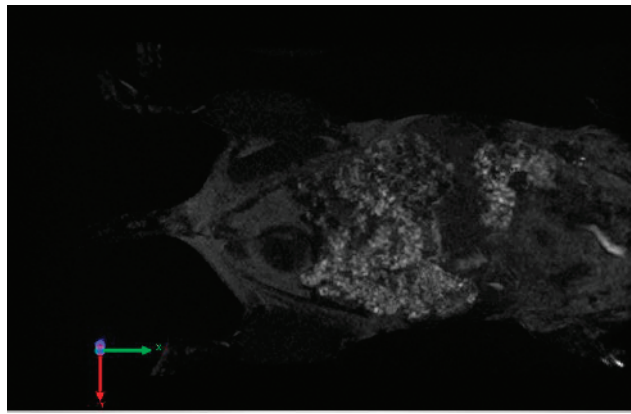
Figure W1. Movie of MRI lymphography in normal mouse. Movie of anesthetized normal mouse during a 10-minute period after Gd-DTPA injection into the dorsal toe of the left hind leg, illustrating slow lymph transport through the lymphatic vessels and LNs to the heart. The movie was created from dynamic scans of the mouse shown in the left column of Figure 2.
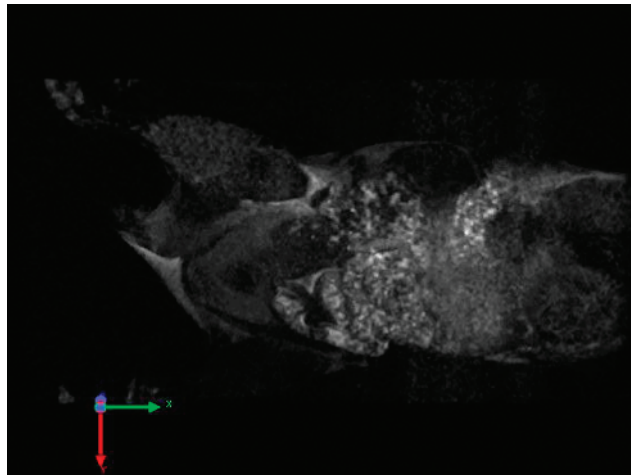

Figure W2. Movie of MRI lymphography in tumor-bearing mouse illustrates the extent of tumor-induced lymph flow. Movie of anesthetized tumor-bearing mouse during a 10-minute period after Gd-DTPA injection into the dorsal toe of the tumor-bearing hind leg. The movie illustrates rapid lymphatic transport to the heart and then on through the vascular circulation. The movie was created from dynamic scans of the mouse shown in the right column of Figure 2.